Numerical simulation of the surface hardening of steel

Jürgen Fuhrmann and Dietmar Hömberg
Weierstrass Institute for Applied Analysis and Stochastics, Berlin, Germany

Keywords *Finite volume, Heat treatment, Steel*

Received November 1997
Revised February 1998
Accepted November 1998

Abstract *We discuss a model that is capable of describing the solid-solid phase transitions in steel. It consists of a system of ordinary differential equations for the volume fractions of the occuring phases coupled with a nonlinear energy balance equation to take care of the latent heats of the phase changes. This model is applied to simulate surface heat treatments, which play an important role in the manufacturing of steel. Two different technologies are considered: laser and induction hardening. In the latter case the model has to be extended by Maxwell's equations. Finally, we present numerical simulations of laser and induction hardening applied to the steel 42CrMo4.*

1. Introduction

In most structural components in mechanical engineering, the surface is particularly stressed. Therefore, the aim of surface hardening is to increase the hardness of the boundary layers of a workpiece by rapid heating and subsequent quenching. This heat treatment leads to a change in microstructure, which produces the desired hardening effect. Typical examples of application are all sorts of cutting tools, (gear-) wheels, driving axles, to name only a few.

In this paper we investigate two different methods for surface hardening: induction and laser hardening.

The mode of operation in induction hardening facilities relies on the transformer principle. A given current density in the coil induces eddy currents inside the workpiece Ω (cf. Figure 1). Because of the Joule effect these eddy currents lead to an increase in temperature in the boundary layers of the workpiece. Then the current is switched off and the workpiece is quenched by spray-water cooling.

When the workpiece is very big or the part of the surface to be hardened has a complicated shape, laser hardening becomes attractive. In this process a laser beam moves along the surface of a workpiece (cf. Figure 2). The laser radiation is absorbed by the workpiece, leading to a rapid heating of its boundary layers. Then, the workpiece is quenched by "self-cooling" of the workpiece.

To increase the scanning width, sometimes the laser beam performs an additional oscillating movement orthogonally to the principal moving direction.

In Section 2 we discuss a mathematical model to describe these heat treatments. Basic ingredients are a rate law to describe the evolution of the phase transitions, which are responsible for the change in hardness of the workpiece. To take care of recalescence effects, this is coupled with an energy balance equation. In addition, we have to describe models for laser radiation and Joule heating respectively. Section 3 is devoted to developing a numerical

International Journal of Numerical Methods for Heat & Fluid Flow, Vol. 9 No. 6, 1999, pp. 705-724.

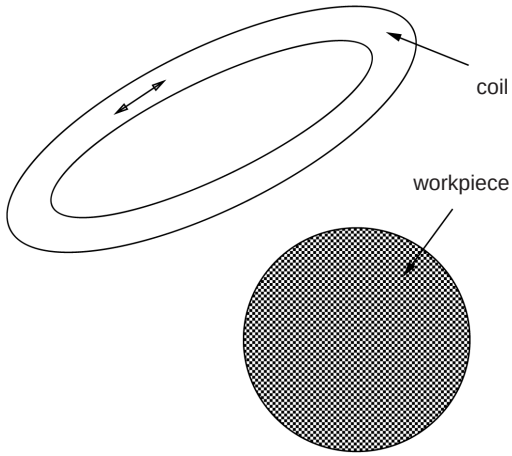

Figure 1.
Sketch of an induction hardening facility

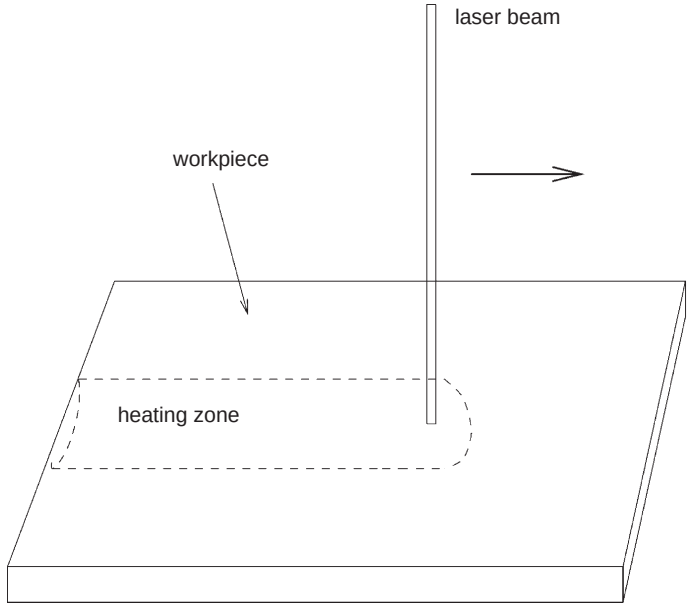

Figure 2.
Sketch of a laser hardening process

algorithm for surface heat treatments. Then, in Section 4 we present numerical simulations for both laser and induction hardening. Finally, in the last section we make some concluding remarks concerning model improvements and further directions of research.

2. Model equations

2.1 The phase transitions

The reason why one can change the hardness of steel by thermal treatment lies in the occuring phase transitions, depicted in Figure 3. At room temperature, in

general, steel is a mixture of ferrite, pearlite, bainite and martensite. Upon heating, these phases are transformed to austenite. Then, during cooling austenite is transformed back to a mixture of ferrite, pearlite, bainite and martensite.

The actual phase distribution at the end of the heat treatment depends on the cooling strategy. In the case of surface hardening, owing to high cooling rates most of the austenite is transformed to martensite by a diffusionless phase transition leading to the desired increase of hardness.

Mathematical models for phase transitions in steel have been considered, e.g.in Hömberg (1995), Hömberg and Sokolowski (1998), Leblond and Devaux (1984), Verdi and Visintin (1987) and Visitin (1987). For a survey on mathematical models for laser material treatments, we refer to Mazhukin and Samarskii (1994).

Before presenting our model we recall some classical approaches for typical phase transitions.

The simplest way to describe diffusive phase transitions like the austenite-pearlite transformation in the isothermal case is the Johnson-Mehl equation

$$p(t) = 1 - e^{-c_1(\theta)t^{c_2(\theta)}}, \tag{2.1}$$

where p is the volume fraction of pearlite and c_1, c_2 are temperature-dependent coefficients, to be determined from time-temperature-transformation diagrams (cf. Hömberg (1996) for details).

In the nonisothermal case, a widely used approach is to apply Scheil's additivity rule (for details and further references we again refer to Hömberg (1996)):

$$\int_0^t \frac{1}{\tilde{\tau}(\theta(\xi), p(t))}\, d\xi = 1. \tag{2.2}$$

Here, $\tilde{\tau}(\theta, p)$ is the time to transform the fraction p to pearlite isothermally at temperature θ. Recently, Fasano and Primicerio (1996) showed that only those functions $\tilde{\tau}$ are admissible for (2.2) that are separable, i.e. that have the form

$$\tilde{\tau}(\theta, p) = \tau_1(\theta) \cdot \tau_2(p). \tag{2.3}$$

Note that c_2 has to be constant, if one wants to utilize (2.1) to compute $\tilde{\tau}$.

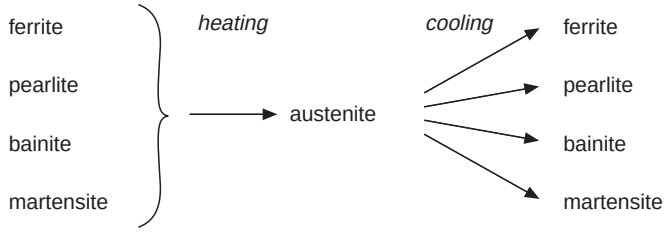

Figure 3.
Possible phase transitions in steel

In view of (2.3), it is easily seen that the additivity rule (2.2) is equivalent to a separable rate law

$$p(t_0) = p_0, \tag{2.4a}$$

$$p_t(t) = f_1(\theta(t))f_2(p(t)). \tag{2.4b}$$

The austenite-martensite phase transition is diffusionless and temperature dependent. Only during nonisothermal stages of a cooling process, can an increase in the martensite fraction be observed.

The easiest way to describe this behaviour is by the rate law

$$m(t_0) = 0, \tag{2.5a}$$

$$m_t(t) = (1 - m(t))f_3(\theta)(\mathcal{H} - \theta_{\sqcup}), \tag{2.5b}$$

where $\mathcal{H}$ is a smooth, monotone approximation of the Heaviside graph. Whenever the temperature is non–decreasing, $-\theta_t \geq 0$ and hence $m_t = 0$.

According to Leblond and Deveaux (1984), the formation of austenite cannot be described by the additivity rule, since for fixed temperature within the transformation range, one can get an equilibrium volume fraction of austenite less than one. Therefore, they propose to use the rate law

$$a(t_0) = 0, \tag{2.6a}$$

$$a_t(t) = \frac{1}{\tau(\theta)} \max\left\{\left(a_{eq}(\theta) - a(t)\right), 0\right\}, \tag{2.6b}$$

with an equilibrium fraction of austenite a_{eq} and a time-constant τ.

Remark 2.1.

(1) Originally, in Leblond and Devaux (1994) the formula

$$a_t(t) = \frac{1}{\tau(\theta)}\left(a_{eq}(\theta) - a(t)\right)$$

was proposed. However, since we want to describe a complete heat treatment cycle, we had to make this modification to ensure that (2.6b) only describes the growth and not the shrinking of austenite.

(2) If one wants to avoid the nonlinearity in θ_t, another way to describe the growth of martensite would be a formula similar to (2.6a-b).

To formulate a general model for phase transitions according to Figure 3, we introduce the following notations:

z_0: volume fraction of austenite,

$z_1, \ldots, z_4$: relative volume fractions of ferrite, pearlite, bainite, martensite, which have been transformed from z_0,

A_s: critical temperature, above which the formation of austenite starts,

M_s: critical temperature, below which the formation of martensite starts ($M_s < A_s$).

We describe the evolution of volume fractions for given temperature evolution $\theta(.)$ by the following initial-value problem:

$$z_0(0) = z_{00} \in (0,1), \tag{2.7a}$$

$$z_i(0) = 0, \qquad i = 1, ..., 4, \tag{2.7b}$$

$$z_{0,t}(t) = \frac{1}{\tau(\theta)} \max\left\{\Big(a_{eq}(\theta(t)) - z_0(t)\Big),\, 0\right\} \mathcal{H}(\theta(t) - A_s) - \sum_{j=1}^{4} z_{j,t}(t) \tag{2.7c}$$

$$z_{i,t}(t) = g_i(t, z(t), \theta(t))\, \mathcal{H}(A_s - \theta(t)), \qquad i = 1, ..., 3, \tag{2.7d}$$

$$z_{4,t}(t) = z_0(t)\mathcal{H}(-\theta_t) g_4(t, z(t), \theta(t))\, \mathcal{H}(M_s - \theta(t)), \tag{2.7e}$$

where we assume

(A1) $\mathcal{H} \in C^\infty(\mathbb{R})$, monotone regularization of the Heaviside graph, satisfying $\mathcal{H}(0) = 0$ (cf. Tiba and Neittaanmaki, 1994, p. 196).

(A2) $a_{eq} \in C^{1,1}(\mathbb{R})$, $a_{eq}(x) \in [0,1]$ for all $x \in \mathbb{R}$.

(A3) $\tau \in C^{1,1}(\mathbb{R})$, $m \le \tau(x) \le M$ for all $x \in I$, and constants $0 < m < M$,

(A4) $g_i \in C^{1,1}(D)$, $i = 1, \ldots, 4$, $D = [0,T] \times [0,1]^5 \times \mathbb{R}$, moreover $0 \le g_i \le M$, for all $(t, z, \theta) \in D$ and a constant $M > 0$.

In Section 4 we will show how this general model can be utilized for the simulation of surface heat treatments.

2.2 Energy balance equation

Neglecting mechanical effects and using Fourier's law of heat conduction, we consider the following heat transfer equation:

$$\rho(\theta)c(\theta)\theta_t - \nabla.\Big(k(\theta)\nabla\theta\Big) = F_1(\theta, z) + F_2, \quad \text{in} \quad Q_T = \Omega \times (0,T). \tag{2.8}$$

Here, $\Omega \subset \mathbb{R}^n$, $n = 2, 3$ is the workpiece and ρ, c, k denote density, specific heat at constant pressure and heat conductivity respectively. The terms F_1, F_2 will take care of the latent heats of the phase transitions and the heat source to be decribed in the following subsections.

We consider a Newton-type boundary condition

$$-k(\theta)\frac{\partial\theta}{\partial\nu} = \gamma(x,t)(\theta - \theta_\Gamma) \quad \text{in} \quad \Sigma_T = \partial\Omega \times (0,T),$$

and the initial condition

$$\theta(.,0) = \theta_0 \quad \text{in} \quad \Omega.$$

Let $L_i > 0$, $i = 0, \ldots, 4$, be the amount of latent heat consumed or released during the phase transitions. Then, F_1 takes the form

$$F_1(\theta, z) = -F_{11}(\theta, z)A(\theta_t) + F_{12}(\theta, z),$$

with

$$A(\theta_t) = -\mathcal{H}(-\theta_t), \tag{2.9a}$$

$$F_{11}(\theta, z) = \rho(\theta)L_4 g_4(t, z, \theta)\mathcal{H}(M_s - \theta), \tag{2.9b}$$

$$F_{12}(\theta, z) = -\frac{\rho(\theta)L_0}{\tau(\theta)} \max\left\{\left(a_{eq}(\theta) - z_0\right), 0\right\} \mathcal{H}(\theta - A_s) + \rho(\theta)\sum_{i=1}^{3} L_i g_i(t, z, \theta)\,\mathcal{H}(A_s - \theta).$$

Hence, in view of (2.7a-e) and (A1)–(A4), latent heat is consumed during the growth of austenite ($z_{0,t} \geq 0$) and released during the formation of ferrite, pearlite, bainite and martensite.

Inserting (2.9a-c) into (2.8), we obtain the following nonlinear energy balance equation:

$$\rho(\theta)c(\theta)\theta_t + F_{11}(\theta, z)A(\theta_t) - \nabla.\left(k(\theta)\nabla\theta\right) = F_{12}(\theta, z) + F_2, \text{ in } Q_T, \tag{2.10a}$$

$$-k(\theta)\frac{\partial\theta}{\partial\nu} = \gamma(x, t)(\theta - \theta_\Gamma) \quad \text{in} \quad \Sigma_T, \tag{2.10b}$$

$$\theta(.,0) = \theta_0 \quad \text{in} \quad \Omega. \tag{2.10c}$$

2.3 Heat source I: laser radiation

Following the lines of Mazhukin and Samarskii (1994), we assume that the laser radiation is absorbed volumetrically by the workpiece, acting as a thermal source of equivalent power. Let the part of the workpiece surface to be hardened lie in the plane $z = 0$ and suppose the laser beam strikes it in the point $(x_0, y_0) \in \partial\Omega$.

Then, the laser radiation penetrates into the workpiece according to the radiation transfer equation

$$\frac{\partial G}{\partial z} = \kappa G, \tag{2.11a}$$

$$G\Big|_{z=0} = \alpha G_f. \tag{2.11b}$$

Here, G is the radiation intensity of the laser beam, G_f the radiation intensity in the focal plane, κ the absorption coefficient and α the absorptivity of the surface, depending on the angle of incidence, the surface constitution (smoothness, cleanliness) and on the temperature.

For constant κ, we have

$$G = \alpha G_f e^{\kappa z}, \qquad z \leq 0. \tag{2.12}$$

G_f is supposed to satisfy a normal distribution law

$$G_f = G_0 e^{-\frac{(x-x_0)^2+(y-y_0)^2}{2R^2}},$$

where R is the radius of the focusing spot and G_0 its intensity in the spot center, i.e.

$$G_0 = P/\pi R^2, \tag{2.13}$$

with the radiation power P.

In applications, the laser beam moves along the workpiece surface according to a curve $t \longrightarrow r(t) \in \mathbb{R}^2,\ t \in [0, T]$, hence we have

$$G_f(x, y, t) = G_0 e^{-\frac{(x-r_1(t))^2+(y-r_2(t))^2}{2R^2}}.$$

The heat source in the case of laser hardening then takes the form

$$F_2 = \kappa G. \tag{2.14}$$

2.4 Heat source II: induction heating

For the sake of simplicity, we assume that the workpiece is translational invariant in the direction of the z-axis with cross section $\Omega \subset \mathbb{R}^2$. In this geometric configuration, it is reasonable to expect that the magnetic field has the form $\vec{H} = (0, 0, h)^T$. Neglecting displacement currents, Maxwell's equations then can be reduced to the following nonlinear parabolic equation (cf. e.g. Clain *et al.*, 1993):

$$(\mu h)_t - \nabla.\left(\frac{1}{\sigma(\theta)}\nabla h\right) = 0, \quad \text{in} \quad Q_T. \tag{2.15a}$$

Here, μ is the magnetic permeability and σ is the electric conductivity. Outside the conductors, h is constant, hence we consider a space-independent Dirichlet boundary condition

$$h(., t) = \varphi(t), \quad \text{in} \quad \Sigma_T, \tag{2.15b}$$

and the initial condition

$$h(., 0) = h_0, \quad \text{in} \quad \Omega. \tag{2.15c}$$

Owing to the Joule effect, the eddy currents induced in the workpiece act as a heat source, which can be described by

$$F_2 = \frac{1}{\sigma(\theta)} \left| \nabla h \right|^2. \tag{2.16}$$

2.5 Summary

The two models for surface hardening under study in this paper correspond to the following sets of equations:

(1) Laser hardening (LH). The model for laser hardening consists of the energy balance (2.10a-c), coupled with the system (2.7a-e) to describe the evolution of the phase fractions and the radiation transfer equation (2.11a,b).

(2) Induction hardening (IH). Here, the energy balance (2.10a-c) and the system (2.7a-f) have to be coupled with Maxwell's equations (2.15a-c).

Well-posedness of the model for laser hardening (LH) can be concluded from Theorem 3.1 in Hömberg (1997). Existence and uniqueness for IH can be proved using a straightforward fixed point argument using Theorem 3.1 in Hömberg (1997) and Theorem 3.1 in Rodrigues (1992).

To maintain the quality of the workpiece surface, it is very important to avoid melting effects. Especially in the case of laser hardening, which is often applied to curved edges, it is a delicate problem to obtain parameters that avoid melting but nevertheless lead to the desired hardening depth.

Mathematically speaking, this corresponds to minimizing the following cost functional

$$J = \int_\Omega \Big(z_4(x, T) - \tilde{m}(x) \Big)^2 dx,$$

subject to the state constraint $\theta \leq \theta_m$ and the state equations (LH). Here, θ_m is the melting temperature and $\tilde{m}$ the desired distribution of martensite.

This control problem has been investigated in Hömberg and Solokowski (1998).

3. Numerical algorithm

To allow for variable time-step sizes, we introduce the following notations:

Let $M \in$ be fixed, $0 = t_0 < t_1 < \ldots < t_M = T$ be a partition of $[0, T]$ and

$$k_m = t_m - t_{m-1}, \qquad 1 \leq m \leq M.$$

Now, we introduce a time-discrete version of the system equations for LH and IH, respectively. We start with approximating the energy balance (2.10a-c): Let $\theta^m : \Omega \longrightarrow \mathbb{R}$ be the solution to

$$\rho(\theta^m)c(\theta^m)\frac{\theta^m-\theta^{m-1}}{k_m}+F_{11}(\theta^m,z^{m-1})A\left(\frac{\theta^m-\theta^{m-1}}{k_m}\right) - \nabla.\left(k(\theta^m)\nabla\theta^m\right)=F_{12}(\theta^m,z^{m-1})+F_2^m,\ \text{in}\ \Omega, \tag{3.1a}$$

$$-k(\theta^m)\frac{\partial\theta^m}{\partial\nu}=\gamma(\theta^m-\theta_\Gamma),\quad \text{in}\quad \partial\Omega, \tag{3.1b}$$

for $1\le m\le M$ and $\theta^0:=\theta_0$. Here, z^m is an approximation of $z(t^m)$, obtained from a fourth order Runge-Kutta method.

In the case of laser hardening, the heat source is discretized by

$$F_2^m=\frac{\kappa}{k_m}\int_{t_{m-1}}^{t_m} G dt.$$

In the case of induction hardening, the situation is more complicated. We have to cope with a rapidly oscillating magnetic field. Hence, φ in (2.15b) takes the form

$$\varphi(t)=\bar{h}\sin 2\pi\omega t, \tag{3.2}$$

with frequencies ω between 10^4 and 10^6Hz.

Therefore, as in Bossavit (1985), Chain *et al.* (1993) or Hope and Kornhuber (1990), we adopt the method of averaging. To this end, we introduce a new time-step size

$$\xi_m=\frac{k_m}{\omega N},\quad N\in\mathbb{N}\quad \text{fixed},$$

where $1/\omega$ is the oscillation period in (3.2). Each time interval $[t_{m-1},t_m]$ is dissected into $\omega\cdot N$ sub–intervals $[t_m^{j-1},t_m^j]$ of length ξ_m, i.e. $t_m^j=t_{m-1}+j\xi_m$. Then, we consider the following time-discrete version of (2.15a-c):

$$\mu\frac{h_m^j-h_m^{j-1}}{\xi_m}-\nabla\left(\frac{1}{\sigma(\theta^{m-1})}\nabla h_m^j\right)=0,\quad \text{in}\quad \Omega, \tag{3.3a}$$

$$h_m^j=\bar{h}\sin(2\pi\omega t_m^j),\quad \text{in}\quad \partial\Omega, \tag{3.3b}$$

for $1\le j\le N$ and $h_m^0:=h_{m-1}$. The system (3.3a,b) is solved until the difference between the averaged gradient of the solution in two consecutive periods becomes small enough (cf. Figure 12). The new value h_m is then obtained by averaging over the last period, and the heat source is given by

$$F_2^m=\frac{1}{\sigma(\theta^m)}|\nabla h^m|^2. \tag{3.4}$$

The space discretizations of both the nonlinear heat conduction problem and the Maxwell equation are carried out with a Voronoi box based vertex centered finite volume method on one-, two- and three-dimensional simplicial meshes. Mesh generation is performed using the grid generator IBG (Schmelzer, 1993).

The solution of the discrete nonlinear heat conduction problem is obtained using Newton-Krylov methods.

When coupled with the time-step control in the right way, Newton's method shows quadratic convergence behaviour, which makes it possible to obtain very exact solutions to the nonlinear problems at low additional cost.

The solution of the linear problems uses the method of conjugated gradients for the Maxwell equation and the BICGstab method for the linear problems occuring during the Newton process in the heat conduction equation, respectively. These methods are preconditioned by incomplete LU factorizations. On rectangular meshes, efficient multigrid preconditioners can be used as well. The development of multigrid preconditioners for unstructured meshes is still going on (cf. Fuhrmann, 1996a).

A detailed description of the nonlinear solution methods can be found in Fuhrmann (1996b), where these methods are applied to a nonlinear porous media flow problem with a structure very similar to the nonlinear heat conduction problem under study in this paper.

4. Simulations for the steel 42 CrMo 4

4.1 Physical data

The numerical simulations are carried out for the steel 42 CrMo 4. Table I depicts its chemical composition. The temperature-dependent coefficients ρ, c, k have been taken from Verein Deutscher Eisenhüttenleute (1968). Here, and in the sequel, we use cubic splines to interpolate between values for different temperatures in order to obtain convergence of the Newton algorithm.

We use (2.6a,b) to describe the formation of austenite during heating. The values for the temperature-dependent coefficients a_{eq} and τ have been taken from Leblond and Devaux(1984). For A_s we use the value

$$A_s = 730\,^{o}\mathrm{C}.$$

According to Figure 3, during cooling four phase transitions may occur. However, in the case of surface hardening we encounter high cooling rates. Hence, it is sufficient to restrict ourselves to the formation of bainite and martensite. The kinetics of these phase transitions can be drawn from the isothermal time-temperature-transformation diagram depicted in Figure 4.

C	Si	Mn	P	S	Cr	Cu	Mo	Ni
0.38	0.23	0.64	0.0019	0.013	0.99	0.17	0.16	0.08

Source: From Vereins Deutscher Eisenhüttenleute (1961)

Table I.
Chemical composition of the steel 42 CrMo 4

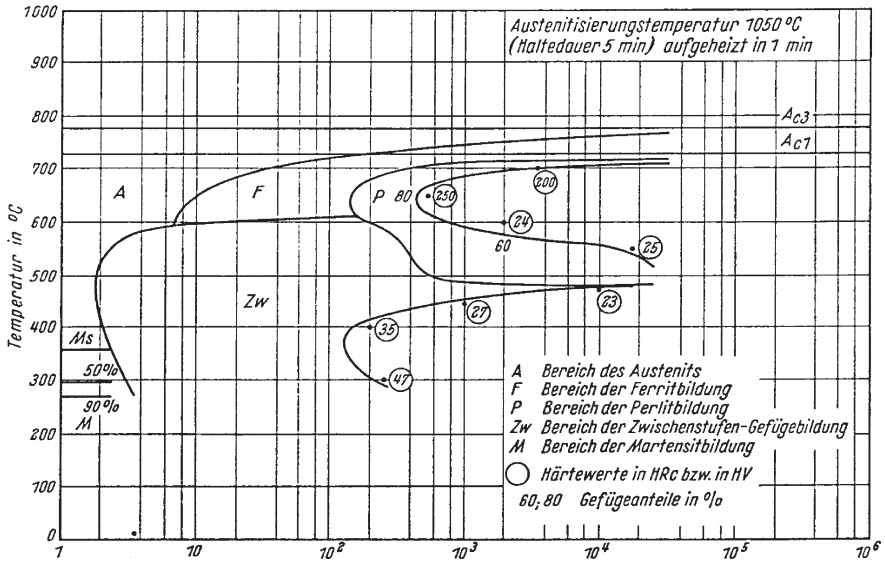

Source: Vereins Deutscher Eisenhütterleute (1961)

Figure 4.
Isothermal time-temperature-transformation diagram for the steel 42CrMo4

For the formation of bainite we make the ansatz

$$b_t = f(b)\, g(\theta), \tag{4.1}$$

where b is the volume fraction of bainite (cf. Section 2.1).

For fixed temperature θ, the curved lines in Figure 4 denote the beginning (t_s) and the end (t_f) of transformation, defined by volume fractions $b = 0.01$ and $b = 0.99$ respectively. Integrating (4.1) keeping θ fixed, we obtain

$$g(\theta) = \frac{1}{t_f - t_s} \int_{0.01}^{0.99} \frac{1}{f(b)}\, db. \tag{4.2}$$

A frequently used ansatz for f is

$$f(b) = b^q\,(1-b)^{1-q}, \qquad \text{and} \quad q \in [0,1]. \tag{4.3}$$

Another approach, using the Johnson-Mehl equation, can be found in Hömberg (1996). Choosing $q = 0$ in (4.3), we obtain

$$g(\theta) = \frac{1}{t_f - t_s} \ln(99)\,. \tag{4.4}$$

The values for t_f and t_s can be drawn from Figure 4. Figure 5 shows the graph of $g(\theta)$.

For the formation of martensite we use the ansatz

$$m_t = (1-m)\, c_m\, \mathcal{H}(-\theta_t)\, \mathcal{H}(M_s - \theta). \tag{4.5}$$

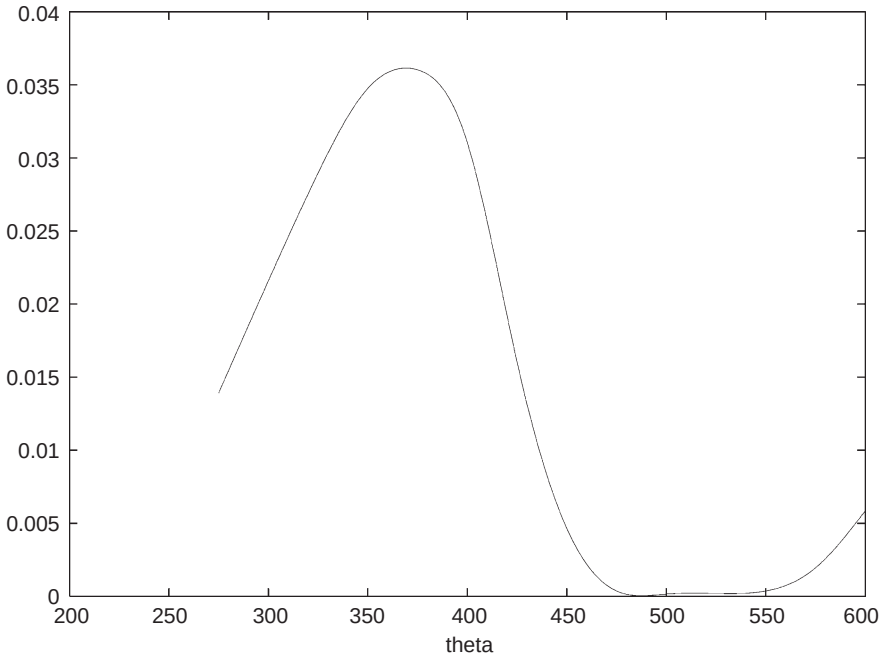

Figure 5.
Graph of the function $g(\theta)$ in (4.4)

The constants c_m and M_s can be identified from the volume fractions of martensite depicted in Figure 4. We chose

$$c_m = 1.4, \qquad M_s = 360^{\circ}\mathrm{C}. \tag{4.6}$$

Replacing $1 - b$ and $1 - m$ with the actual volume fraction of austenite, we end up with the following initial-value problem:

$$a(0) = b(0) = m(0) = 0, \tag{4.7a}$$

$$a_t(t) = \frac{1}{\tau(\theta(t))} \max\left\{a_{eq}(\theta(t)) - a(t)\,,\, 0\right\}\mathcal{H}(\theta - A_s) - b_t(t) - m_t(t), \tag{4.7b}$$

$$b_t(t) = a(t)\, g(\theta(t)), \tag{4.7c}$$

$$m_t(t) = a(t)\, c_m \mathcal{H}(-\theta_t(t))\mathcal{H}(M_s - \theta(t)). \tag{4.7d}$$

In our simulations we assume further that the latent heat L is the same for all the phase transitions, namely

$$L = 82 \left[\frac{J}{g}\right]. \tag{4.8}$$

Then, the functions F_{11} and F_{12} in (2.9b,c) take the form

$$F_{11}(\theta, a, b, m) = \rho(\theta)\, L\, c_m\, a\, \mathcal{H}(M_s - \theta), \tag{4.9}$$

$$F_{12}(\theta, a, b, m) = -\frac{\rho(\theta)\, L}{\tau(\theta)} \max\Big\{ a_{eq}(\theta) - a, 0 \Big\} \mathcal{H}(\theta - A_s) + \rho(\theta) L a g(\theta). \tag{4.10}$$

4.2 Numerical results for laser hardening

A disadvantage of laser hardening is that no additional spray water cooling can be applied to support the quenching process. This is reflected in numerical simulations: to obtain the desired hardening effect by the formation of martensite, one has to make full 3-d calculations, otherwise not enough heat can be carried off.

We simulate the hardening along a strip around the y-axis on the upper face ($z = 0$) of the cube $\bar{\Omega} = [-2.5, 2.5] \times [0, 10.0] \times [-1.0, 0]$. The values for the physical parameters used in these calculations can be found in Table II. They correspond to a 2.8kW Nd:YAG-laser. Since the main quenching effect is the self-cooling of the workpiece, we assume $\gamma \equiv 0$ in (3.1b), i.e. a homogeneous Neumann boundary condition for θ.

The scanning width s is twice the amplitude of the oscillations orthogonally to the moving direction related to the spotcenter, and f their frequency. The remaining parameters are explained in Section 2.3. The absorption coefficient κ and the absorptivity α have been gauged by comparison with measured hardening profiles.

Figure 6 shows the time evolution at the point $x = (0.0, 1.0, -0.01) \in \Omega$. Owing to the oscillations of the laser beam, the point is heated by steps. Austenite is formed, and during cooling this austenite is transformed to martensite and a fairly small amount of bainite. In the course of martensite growth, the cooling process is slowed down by the release of latent heat.

Figure 7 depicts the temperature distribution on the upper surface of Ω at time $t = 3$s. The variety of possible hardening profiles and the interplay between the control parameters R and v is illustrated in Figures 8 and 9. The typical hardening depth is between 0.1 and 1mm. To improve the visualization, we enhanced the effect by increasing κ and α. To avoid surface melting this

Description	Denotation	Value (range)	Unit
Radius of focusing spot	R	0.25, . . ., 0.9	cm
Radiation power	P	2,800	W
Absorption coefficient	κ	60.0	1/cm
Absorptivity	α	0.3	
Laser beam velocity	v	50, . . ., 150	cm/min
Scanning width	s	0.0, . . ., 1.3	cm
Frequency of oscillation	f	175	Hz

Table II.
Physical data for laser hardening

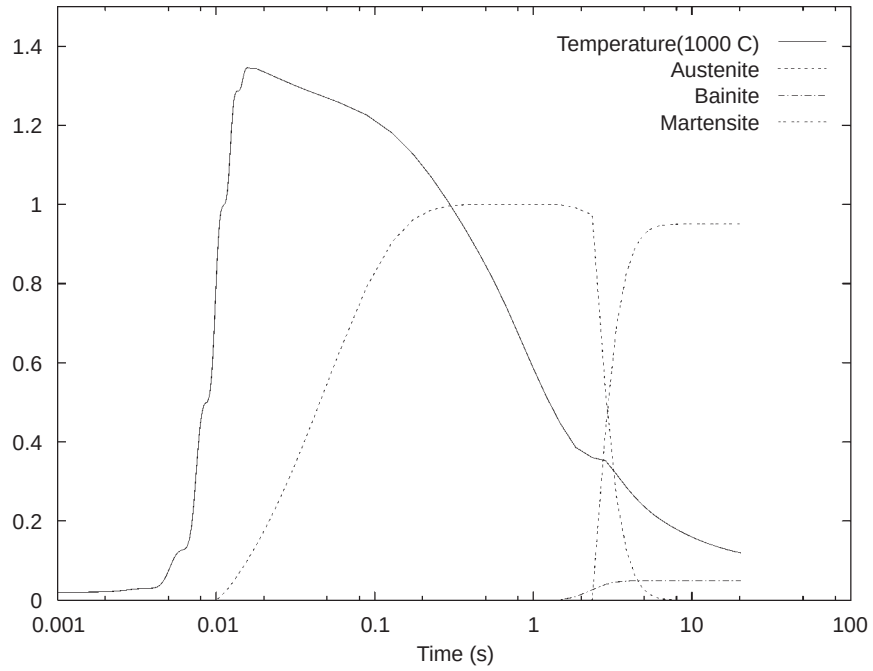

Figure 6.
Time evolution of temperature, austenite, bainite and martensite fraction for x=(0.0, 1.0, –0.01) $\in \Omega$

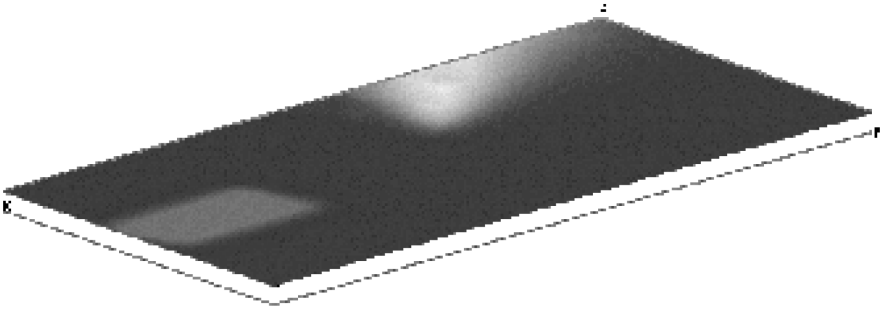

Figure 7.
Temperature distribution on the upper workpeice surface at time t = 3.0s

had to be compensated by an increase in laser beam velocity. That is why the velocities are greater than in Table II. The profiles in Figure 8 are obtained without oscillations of the laser beam. The widening of the hardness profile has been achieved by increasing the radius R of the focusing spot. Since increasing R leads to a decrease of the radiation intensity G_0 (cf. (2.13)), the velocity has to be reduced in order to get the same depth of the hardening profile.

In Figure 9, the spot radius is the same as in Figure 8(a). Here, the widening of the profile has been achieved by letting the laser beam oscillate orthogonally to the moving direction. While the amplitude is the same in (a) and (b), the kind of oscillation is different. The sawtooth form in Figure 9(a) leads to a uniform heating along the hardening strip, while the sinusoidal oscillations in Figure

9(b) preferentially heat the boundary of the strip. This leads to a further widening of the hardening profile, but to obtain the same profile depth as before, the velocity has to be reduced.

To demonstrate that our model is able to predict the hardening profile also quantitatively, we compare our results with measurements carried through by INPRO GmbH, Berlin. Figure 10 shows the relationship between measured hardening depth and laser velocity. The curve endings for low velocities indicate the beginning of surface melting. Below, the corresponding simulated diagram is depicted, using the parameters of Table II.

We define the depth of the hardening profile to be the maximal distance from the surface, where the volume fraction of martensite is greater than or equal to 90 per cent. Although the exact shape of the curves is different from the measured ones, they show the same increase with decresing velocity. For small velocities the relationship between hardening depth and velocity tends to become independent of the focus radius. The maximal absolute error is approximately 0.1mm.

A more detailed comparison would require more refined metallurgical measurements and is beyond the scope of this paper.

4.3 Numerical results for induction hardening

For the magnetic permeability we use the value

$$\mu = 4\pi \cdot 10^{-9} \quad \frac{V\,s}{A\,cm}.$$

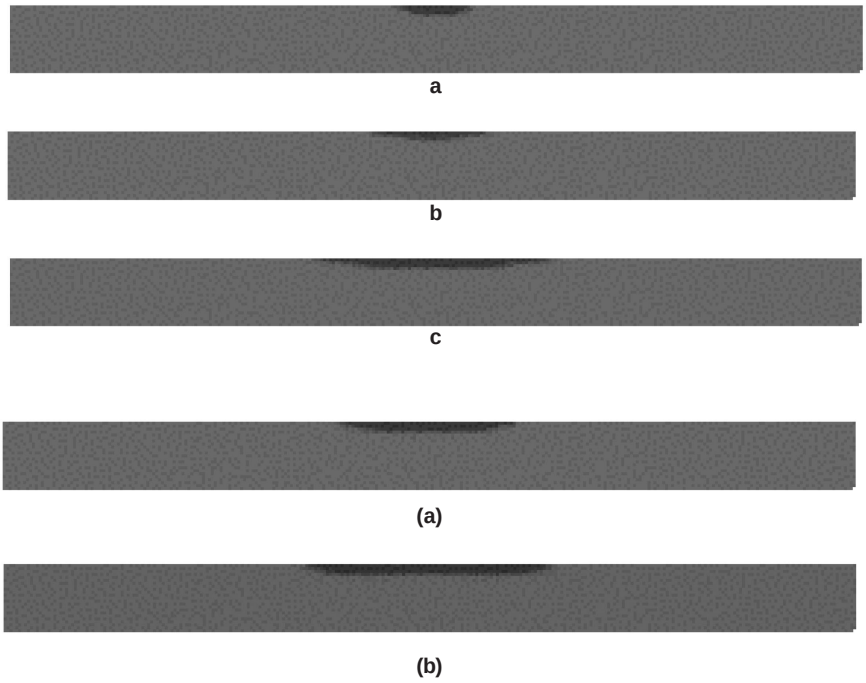

Figure 8.
Hardening profile at y = 1.0, no oscillations; (a) R = 0.25cm, v = 150cm/s; (b) R = 0.5cm, v = 50cm/s; (c) R = 0.9cm, v = 50cm/s;

Figure 9.
Hardening profile at y = 1.0; (a) sawtooth oscillations, R = 0.25cm, s = 1.3cm, v = 100cm/s; (b) sinusoidal oscillations, R = 0.25cm, s = 1.3cm, v = 80cm/s;

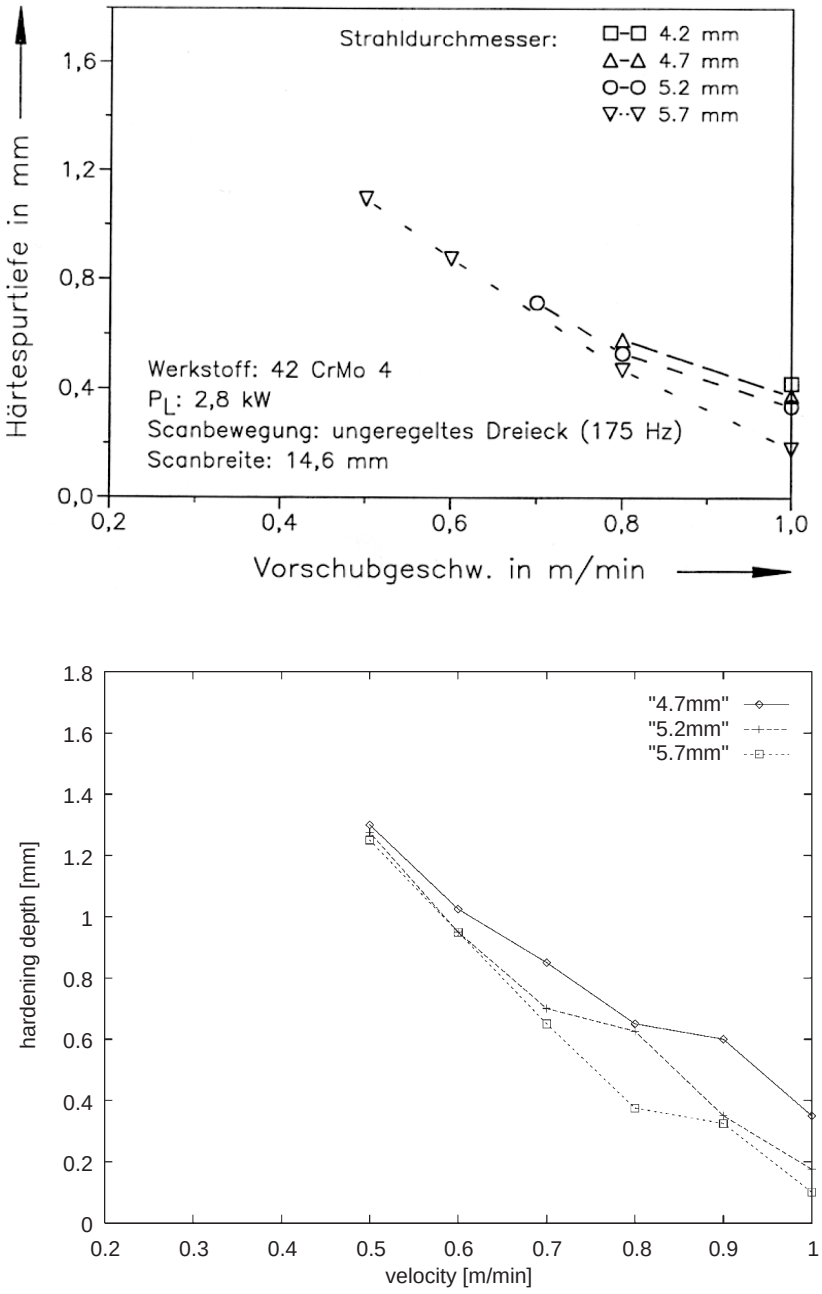

Figure 10.
Measured hardening depth against velocity of the laser beam (INPRO GmbH, Berlin), above, and the corresponding numerical simulations, below

The electric conductivity is assumed to be temperature-dependent, i.e.

$$\sigma(\theta) = \frac{1}{c_1 + c_2\theta + c_3\theta^2 + c_4\theta^3} \quad \frac{1}{\Omega\, cm},$$

with $c_1 = 4.9656 \cdot 10^{-5}$, $c_2 = 8.4121 \cdot 10^{-8}$, $c_3 = -3.7246 \cdot 10^{-11}$, $c_4 = 6.1960 \cdot 10^{-15}$ (cf. Chain *et al.*, 1993).

We call t_1 the time, until when the workpiece is heated by the eddy currents, and assume that the water cooling starts at t_1. Hence, the Dirichlet condition in (2.15b) takes the form

$$\varphi(t) = \begin{cases} \bar{h}\sin(2\pi\omega t), 0 \le t < t_1, \\ 0, \qquad\qquad t \ge t_1, \end{cases} \tag{4.11}$$

with $\bar{h} = 1.5 \cdot 10^3$A/cm. The heat exchange coefficient γ in (2.10b) has been chosen according to Hömberg (1996) as

$$\gamma(t) = \begin{cases} 0, \quad 0 \le t < t_1, \\ 2.8, t \ge t_1, \end{cases}$$

expressed in J/cm^{2}sK. We simulate the surface hardening of a "very thick" gear–wheel. For symmetry reasons, the domain can be reduced to the sector Ω depicted in Figure 11.

As explained in Section 3, we have to work with two time-scales. In each time-step k_m we solve (3.3a,b), until the difference between the averaged gradient of the solution in two consecutive periods becomes small enough (see Figure 12).

In two space dimensions, the magnetic field is constant outside Ω. Therefore, geometric effects like a varying distance between the workpiece Ω and the coil (cf. Figure 1) cannot be taken into account. Thus, the important control parameters in our simulations are the frequency ω and the heating time t_1.

Figure 13 depicts the result of a simulation at time $t = 0.42$s. The left gear-wheel shows the temperature distribution while the right one represents the distribution of phases.

Figure 14 shows the influence of the skin effect on the hardening depth. With growing frequency, the hardening depth decreases.

These are only qualitative results. To obtain quantitative predictions, the amplitude $\bar{h}$ in (4.11), which we have estimated numerically in order to get visible hardening depths, has to be gauged by comparison with experiments.

5. Conclusions

We have investigated a mathematical model for laser and induction surface hardening, including the occuring phase transitions that produce

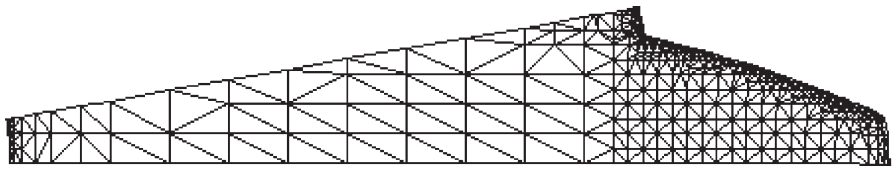

Figure 11.
Computational domain

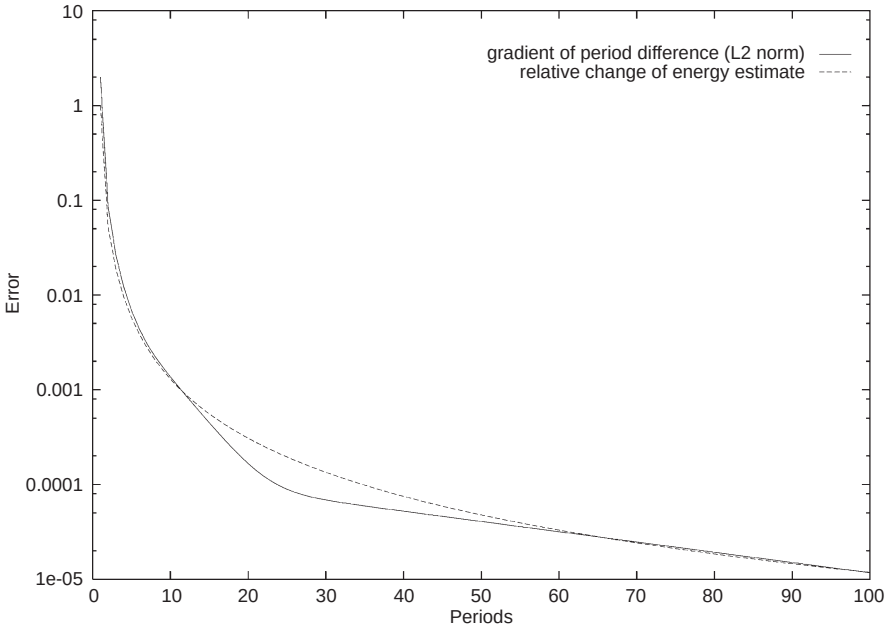

Figure 12.
Difference between the averaged gradient of the solution in two consecutive periods in different norms and relative change of energy estimate, θ fixed

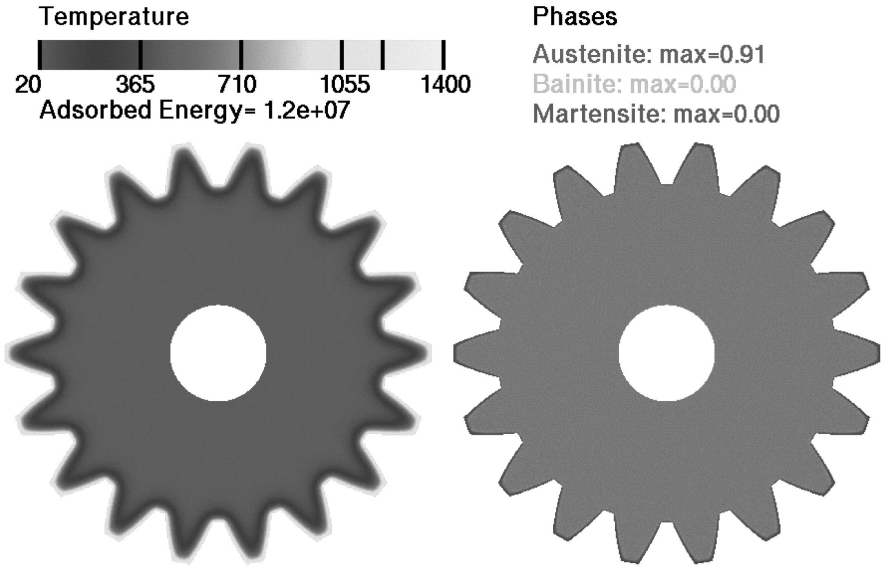

Figure 13.
Result of the numerical simulation at time t = 0.42s, t_1 = 0.48s, ω =10^5Hz

the hardening effect. In the simulations presented here, the formation of bainite is negligible (always less than 5 per cent). However, if workpieces with more complicated geometries are considered, where the heat cannot be carried off fast enough, the growth of bainite becomes important.

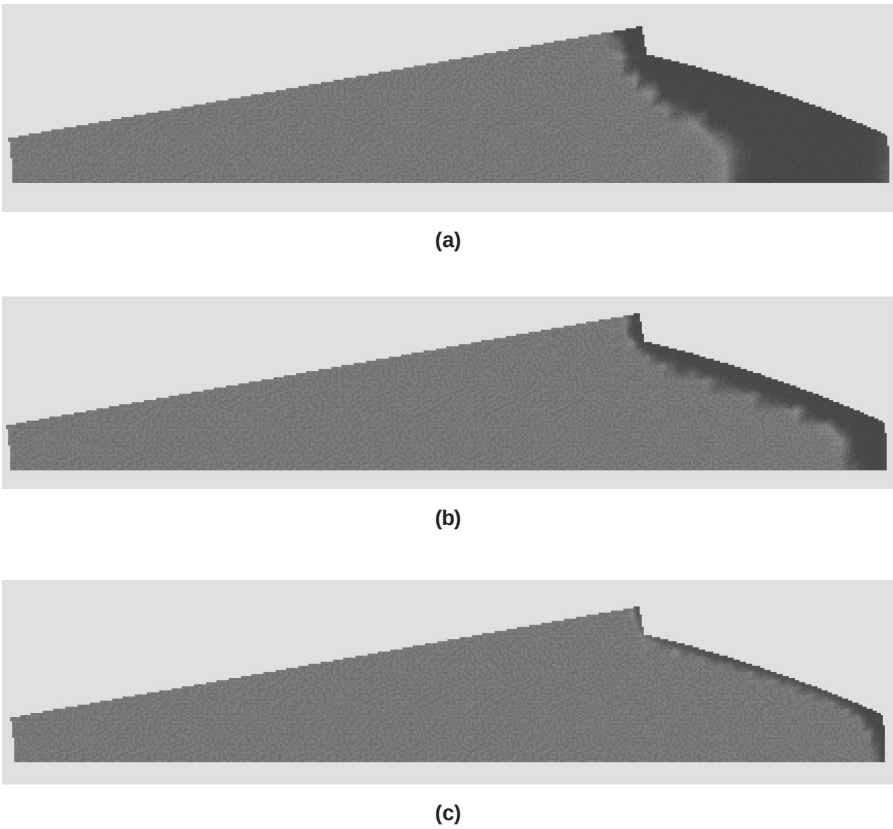

Figure 14.
Influence of the skin effect on the hardening depth: (a) $\omega = 10^4$Hz, t_1 = 3.3s; (b) $\omega - 10^5$Hz, t_1 = 0.48s; (c) $\omega = 10^6$Hz, t_1 =0.06s

Concerning laser hardening, a comparison between Figures 8 and 9 shows that instead of simply increasing the spot radius, the widening of a hardness profile can be achieved more efficiently if the beam oscillates orthogonally to the moving direction.

A comparison with measurments shows that the depth of the hardening profile can be predicted with a maximal error of approximately 0.1mm.

For more complex geometries, the estimation of parameters for laser hardening is a difficult task. Hence, an important direction for further research is the development of numerical optimization strategies.

In the case of induction hardening, the numerical results show all the features that are observed in practice. However, for a quantitative comparison with measurements, one should be able to account for varying distance between coil and workpiece. This problem cannot be treated in the 2D approximation of Maxwell's equations considered here, since in this case the magnetic field is space-independent outside the workpiece.

Therefore, the development of efficient solvers for Maxwell's equations in three space-dimensions is another important direction of further research.

References

Bossavit, A.(1985), "Free boundaries in induction heating", *Control Cybern.*, Vol. 14, pp. 69-96.

Clain, S. *et al.* (1993), "Numerical modelling of induction heating for two-dimensional geometries", *Math. Models Methods Appl. Sci.*, Vol. 3 No. 6, pp. 271-81.

Energie- und Betriebswirtschaftsstelle des Vereins Deutscher Eisenhüttenleute (1968), *Anhaltszahlen für die Wärmewirtschaft in Eisenhüttenwerken*, Verlag Stahleisen mbH, Düsseldorf.

Fasano, A. and Primicerio, M. (1996), "An analysis of phase transition models", *European J. Appl. Math.*, Vol. 7, pp. 439-51.

Fuhrmann, J. (1996a), "On numerical solution methods for nonlinear parabolic problems", *Proceedings of the 1st GAMM-Seminar on Modelling and Computation in Environmental Sciences*, Stuttgart, 12-13 October 1995, to appear in *Notes Numer. Fluid Mech.*

Fuhrmann, J. (1996b), "Outlines of a modular algebraic multigrid method", in Axelsson, O. and Polman,B. (Eds), *Proceedings of the Conference on Algebraic Multilevel Iteration Methods*, Nijmegen, 13-15 June.

Hömberg, D. (1995), "A mathematical model for the phase transitions in eutectoid carbon steel", *IMA J. Appl. Math.*, Vol. 54, pp. 31-57.

Hömberg, D. (1996), "A numerical simulation of the Jominy end-quench test", *Acta Mater.*, Vol. 44, pp. 4375-85.

Hömberg, D. (1997), "Irreversible phase transitions in steel", *Math. Methods Appl. Sci.*, Vol. 20, pp. 59-77.

Hömberg, D. and Sokolowski, J. (1998), "Optimal control of laser hardening", *Adv. Math. Sci. Appl.*, Vol. 8, pp. 911-28.

Hoppe, R.H.W. and Kornhuber, R. (1990), "Multi-grid solution of two coupled Stefan equations arising in induction heating of large steel slabs", *Internat. J. Numer. Methods Engrg*, Vol. 30, pp. 779-801.

Leblond, J.-B. and Devaux, J. (1984), "A new kinetic model for anisothermal metallurgical transformations in steels including effect of austenite grain size", *Acta Met.*, Vol. 32, pp. 137-46.

Max-Planck-Institut für Eisenforschung und der Werkstoffausschuss des Vereins Deutscher Eisenhüttenleute (1961), *Atlas zur Wärmebehandlung der Stähle, Teil I+II*, Verlag Stahleisen mbH, Düsseldorf.

Mazhukin, V.I. and Samarskii, A.A. (1994), "Mathematical modeling in the technology of laser treatments of materials", *Surveys Math. Indust.*, Vol. 4, pp. 85-149.

Rodrigues, J.-F. (1992), "A nonlinear parabolic system arising in thermomechanics and in thermomagnetism", *Math. Models Methods Appl. Sci.*, Vol. 2, pp. 271-81.

Schmelzer, I. (1993), *3D Anisotropic Grid Generation with Intersection-based Geometry Interface*, IMA preprint series no. 1180.

Tiba, D. and Neittaanmaki, P. (1994), "Optimal control of nonlinear parabolic systems", *Monographs Textbooks Pure Appl. Math.*, Vol. 179, M. Dekker, New York, NY.

Verdi, C. and Visintin, A. (1987), "A mathematical model of the austenite-pearlite transformation in plain steel based on the Scheil's additivity rule", *Acta Metall.*, Vol. 35 No. 11, pp. 2711-17.

Visintin, A. (1987), "Mathematical models of solid-solid phase transitions in steel", *IMA J. Appl. Math.*, Vol. 39, pp. 143-57.